

# Quantized Spin-Hall Conductivity in Altermagnet $\text{Fe}_2\text{Te}_2\text{O}$ with Mirror-Spin Coupling

Run-Wu Zhang,<sup>1,2,\*</sup> Chaoxi Cui,<sup>1,2,\*</sup> Yang Wang,<sup>1,2</sup> Jingyi Duan,<sup>1,2</sup> Zhi-Ming Yu,<sup>1,2,†</sup> and Yugui Yao<sup>1,2,‡</sup>

<sup>1</sup>Key Lab of advanced optoelectronic quantum architecture and measurement (MOE),  
Beijing Key Lab of Nanophotonics & Ultrafine Optoelectronic Systems,  
and School of Physics, Beijing Institute of Technology, Beijing 100081, China

<sup>2</sup>International Center for Quantum Materials, Beijing Institute of Technology, Zhuhai, 519000, China  
(Dated: March 17, 2025)

Due to spin-orbit coupling (SOC), crucial for the quantum spin Hall (QSH) effect, a quantized spin-Hall conductivity has not yet been reported in QSH insulators and other realistic materials. Here, we tackle this challenge by predicting robust quantized spin-Hall conductivity in monolayer  $\text{Fe}_2\text{Te}_2\text{O}$ . The underlying physics originates from the unrecognized mirror-spin coupling (MSC), which couples spin-up and spin-down states into two orthogonal mirror eigenstates. We show that the MSC can naturally emerge in the two-dimensional altermagnets with out-of-plane Néel vector and horizontal mirror. A remarkable consequence of the MSC is that it can dramatically weaken the spin hybridization of the altermagnetic materials when SOC is included. When SOC is neglected,  $\text{Fe}_2\text{Te}_2\text{O}$  is an altermagnetic Weyl semimetal with MSC. With SOC, it evolves into the first material candidate for magnetic mirror Chern insulator. Remarkably, under the protection of MSC, the spin hybridization of both bulk and topological edge states in  $\text{Fe}_2\text{Te}_2\text{O}$  with SOC at low energy is negligible. As a consequence, a quantized spin-Hall conductivity emerges within the bulk band gap of the system. By unveiling a novel effect, our findings represent a significant advancement in spin Hall transport, and broaden the material candidates hosting intriguing altermagnetic phenomena.

**Introduction.**— Topological materials have garnered significant interest and rapidly advanced in both fundamental research and practical applications [1–12]. These systems are mathematically characterized by quantized topological charge, such as the Chern number in quantum anomalous Hall (QAH) insulators and the  $Z_2$  invariant in quantum spin Hall (QSH) insulators. Many efforts have been made to unveil quantized physical quantities associated with topological charge [13–15]. A typical example is the Hall conductivity of QAH insulators, which is directly proportional to the Chern number of the systems and thus becomes quantized [16].

Similarly, one may expect that a quantized spin-Hall conductivity could be achieved in QSH insulators. However, this is generally impossible due to a fundamental restriction [17]. To realize a significant QSH effect, the system should exhibit strong spin-orbit coupling (SOC) [18, 19]. However, the SOC will hybrid the spin-up and spin-down states, making each of the topological helical edge states in the QSH insulator lack persistent spin polarization. Therefore, for a four-terminal setup, which is used to measure the spin-Hall transport, the spin-Hall conductivity of the QSH insulator generally is not a constant within the bulk band gap [17]. Consequently, while quantized spin-Hall conductivity can be found in many simplified effective models [20–23], where the spin is a conserved quantity, it remains a challenge to identify material candidates that host this quantized effect, as SOC is an intrinsic property of realistic materials.

Here, we address this challenge by going beyond the traditional QSH effect, circumventing this fundamental restriction with the help of an unrecognized coupling effect. The physics of this work is to explore a two-

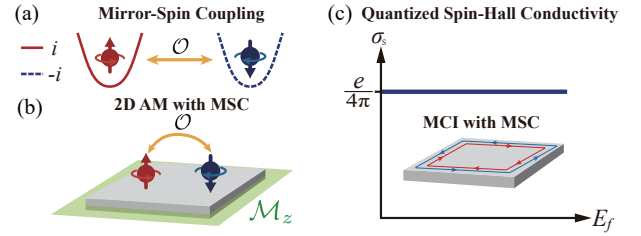


FIG. 1. (a) Illustration of MSC. With MSC, the two symmetry-connected bands with opposite spin polarizations are endowed with opposite mirror eigenvalues. (b) 2D AM systems with out-of-plane Néel vector and horizontal mirror naturally have MSC. (c) An MCI with MSC hosts counter-propagating topological edge states comprising electrons of opposite but persistent spin polarization, leading to quantized spin-Hall conductivity. In (a), solid and dashed lines respectively show the opposite mirror eigenvalues.

dimensional (2D) mirror Chern insulator (MCI) with mirror-spin coupling (MSC). For a 2D system with a horizontal mirror plane ( $\mathcal{M}_z$ ), each energy band is endowed with a certain mirror eigenvalue. The MSC effect here means that the spin polarization of the states in each band depends on the mirror eigenvalue of the band, and the two symmetry-connected bands with different mirror eigenvalues exhibit opposite spin polarizations, as shown in Fig. 1(a). Via symmetry analysis, we first show that the MSC naturally appears in the recently proposed altermagnetic (AM) systems [24–31] with out-of-plane Néel vector and horizontal mirror [see Fig. 1(b)]. In AM materials, the spin is a conserved quantity, but is split in momentum space by the Zeeman effect, leading to various unique properties [32–41]. A major advantage of

altermagnets is the decoupling of spin-up and spin-down states. However, this advantage generally is diminished by the SOC effect. Surprisingly, we find that the MSC can significantly reduce the SOC-induced spin hybridization, allowing the SOC systems still to have persistent spin polarization. Therefore, for an AM material with MSC, when it evolves into an MCI under the SOC effect, we will obtain an MCI with MSC (see Fig. 1). Then, one can expect that the two counter-propagating topological edge states of this novel MCI should exhibit opposite but persistent spin polarization, leading to quantized spin-Hall conductivity in the bulk band gap, as illustrated in Fig. 1(c).

Based on first-principle calculations, we demonstrate our ideas by predicting the monolayer  $\text{Fe}_2\text{Te}_2\text{O}$ . Without SOC, the  $\text{Fe}_2\text{Te}_2\text{O}$  is an AM material with MSC, and has two ideal Weyl points (WPs) in each spin channel around the Fermi level. Due to MSC, the spin-opposite WPs have different  $\mathcal{M}_z$  eigenvalues  $m_z = \pm i$ . Particularly, they are well separated from each other in  $k$ -space, and also are isolated from other bands in energy. When SOC is included, all the WPs are gapped out. The gapped WPs with  $m_z = i$  and  $m_z = -i$  respectively give a Chern number of 1 and  $-1$ , making monolayer  $\text{Fe}_2\text{Te}_2\text{O}$  the first material candidate of magnetic MCI. Notably, the spin hybridization of both bulk and topological edge states in  $\text{Fe}_2\text{Te}_2\text{O}$  with SOC at low energy is negligible, as protected by MSC. As a consequence, a quantized spin-Hall conductivity indeed is observed in the bulk band gap of the system. Our work advances our fundamental understanding of topological phases in AM systems, and paves the way for the development of quantized spintronics devices.

*MSC in Altermagnets.*— We begin by demonstrating that the MSC effect can naturally arise in the 2D AM materials with out-of-plane Néer vector and horizontal mirror, as shown in Fig. 1(b).

The symmetry of AM systems is described by the spin space group (SSG) [42–47]. Since the spin direction and spatial coordinates in SSG vary independently, the  $\mathcal{M}_z$  in this AM system can be written as  $\mathcal{M}_z = \{M_z^s || M_z^l\} = \{C_{2z}^s P^s || M_z^l\}$ , where  $C_{2z}^s$ ,  $P^s$  and  $M_z^s$  represent the two-fold rotation, inversion and horizontal mirror acting on spin (lattice) space, respectively. Notice that in spin space,  $P^s$  is identical to the identity operator  $E^s$ . Therefore, we can express the mirror symmetry as  $\mathcal{M}_z = \{C_{2z}^s || M_z^l\}$ , with eigenvalues being  $m_z = \pm i$  due to the presence of spin operator. Besides, the system must have (at least) one operator, denoted as  $\mathcal{O}$ , that connects the two different spins. The  $\mathcal{O}$  can be either  $\mathcal{O} = \{C_{2,\parallel}^s || O^l\}$  where  $C_{2,\parallel}^s$  is an arbitrary two-fold in-plane rotation on spin, or  $\{E || O^l\} \mathcal{T} = \{C_{2,\parallel}^s || O^l\} * \{C_{2,\parallel}^s || E^l\} \mathcal{T}$  with  $\{C_{2,\parallel}^s || E^l\} \mathcal{T}$  being an intrinsic symmetry of AM. Here,  $\mathcal{T}$  is the time-reversal symmetry.

For simplicity, we use point spin group symmetry to discuss the MSC effect. Since  $C_{2,\parallel}^s$  anticommutes with  $C_{2z}^s$ , and all symmorphic operators  $O^l$  commute with  $M_z^l$ , we always have

$$\{\mathcal{M}_z, \mathcal{O}\} = 0, \quad (1)$$

for  $\mathcal{O} = \{C_{2,\parallel}^s || O^l\}$ , and

$$[\mathcal{M}_z, \mathcal{O}] = 0, \quad (2)$$

for  $\mathcal{O} = \{E || O^l\} \mathcal{T}$ .

The Bloch states of the AM system in the Brillouin zone (BZ) can be chosen as the eigenstates of  $\mathcal{M}_z$ , which we denoted as  $|m_z, \mathbf{k}_{\uparrow(\downarrow)}\rangle$  with  $m_z = \pm i$ , and  $\mathbf{k}_{\uparrow(\downarrow)}$  representing the momentum of the spin-up (spin-down) state. From Eq. (1), one finds that

$$\mathcal{M}_z \mathcal{O} |\pm i, \mathbf{k}_{\uparrow(\downarrow)}\rangle = \mp i \mathcal{O} |\pm i, \mathbf{k}_{\uparrow(\downarrow)}\rangle, \quad (3)$$

for both  $\mathcal{O} = \{C_{2,\parallel}^s || O^l\}$  and  $\mathcal{O} = \{E || O^l\} \mathcal{T}$ . This indicates that  $\mathcal{O} |\pm i, \mathbf{k}_{\uparrow(\downarrow)}\rangle = |\mp i, \mathbf{k}'_{\uparrow(\downarrow)}\rangle$ , where  $\mathbf{k}' = O^l \mathbf{k}$  or  $\mathbf{k}' = -O^l \mathbf{k}$  (when  $\mathcal{O}$  includes  $\mathcal{T}$ ). Consequently, the symmetry-connected spin-up and spin-down bands should have opposite mirror eigenvalues, resulting in the MSC in AM systems.

The MSC can lead to an important consequence for the AM systems. Most of the unique phenomena in AM systems arise from the decoupling of the spin-up and spin-down states, a feature that can be diminished by SOC. However, the MSC provides a protection for this decoupling, as  $\mathcal{M}_z = \{M_z^s || M_z^l\}$  persists even under the influence of SOC. This protection is most significant when the electronic bands in each spin channel near the Fermi level share the same mirror eigenvalues, while all other bands lie far away from the Fermi level [see Fig. 2(c)]. In such a case, the hybridization between the spin-up and spin-down states at low energies is negligible. As a result, systems with MSC can maintain persistent spin polarization despite the presence of SOC. This means that the MSC systems can be ideal platforms for combining two conflicting effects: SOC and spin decoupling (persistent spin texture), which is a critical challenge in the field of spintronics [48–53], and can effectively address the aforementioned fundamental restriction for achieving quantized spin Hall conductivity (provided the system is a magnetic MCI).

We note that Eqs. (1-3) also may be satisfied in certain SOC systems. However, this can not guarantee these SOC systems to have MSC, due to the spin hybridization. To achieve MSC in SOC systems, the practical way is finding AM materials satisfying Eqs. (1-3) and maintaining a clean band structure around the Fermi level.

*MSC material candidates.*— In physics, many promising concepts have made significant theoretical progress.

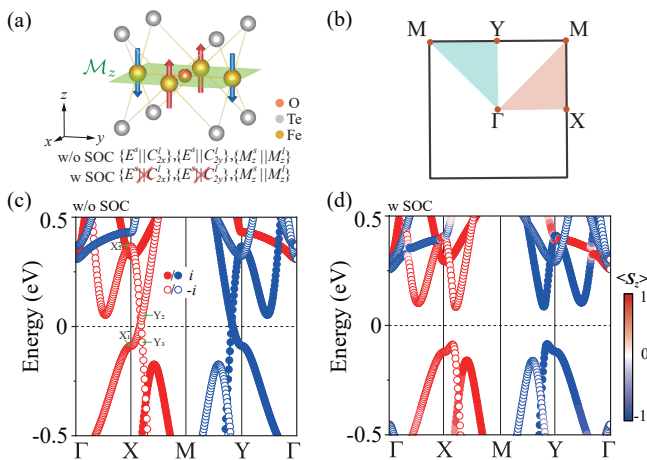


FIG. 2. (a) shows the relaxed geometry of monolayer Fe<sub>2</sub>Te<sub>2</sub>O, which exhibits out-of-plane Néel vector and  $\mathcal{M}_z$ . The  $\mathcal{M}_z$  is always a symmetry operator of Fe<sub>2</sub>Te<sub>2</sub>O, regardless of the SOC. (b) Brillouin zone (BZ) of Fe<sub>2</sub>Te<sub>2</sub>O. (c-d) Electronic band structure of Fe<sub>2</sub>Te<sub>2</sub>O (c) without (w/o) and (d) with (w) SOC. In (c), the bands in spin-up and spin-down channels are plotted as red and blue curves, respectively. In (d), the colors indicate out-of-plane spin polarization ( $s_z$ ). In (c-d), solid and hollow circles respectively denote the states with  $\mathcal{M}_z = +i$  and  $\mathcal{M}_z = -i$ .

However, turning these ideas into practical material systems depends heavily on the discovery of suitable candidate materials. Here, we demonstrate that monolayer Fe<sub>2</sub>Te<sub>2</sub>O is a candidate with MSC.

Monolayer Fe<sub>2</sub>Te<sub>2</sub>O can be obtained through mechanical exfoliation from bulk Fe<sub>2</sub>Te<sub>2</sub>O [54], which is a homologue of experimentally synthesized materials: layered iron oxytelluride family BaFe<sub>2</sub>Ch<sub>2</sub>O (where Ch represents a chalcogen) [55–57]. The crystal structure of the monolayer Fe<sub>2</sub>Te<sub>2</sub>O consists of three atom layers arranged in the sequence Te-(Fe-O)-Te, as shown in Fig. 2(a). The two Fe atoms and one O atoms lie in the same plane, sandwiched between the two Te atomic layers. The crystal lattice belongs to the space group P4/mmm (No. 123), with an optimized lattice constant of  $a = b = 4.03$  Å. Phonon spectrum and molecular dynamics simulations further confirm the structural stability [54], indicating that Fe<sub>2</sub>Te<sub>2</sub>O is robust enough to form a freestanding 2D material. By comparing the energies of several possible magnetic configurations, we confirm that the ground state of the monolayer Fe<sub>2</sub>Te<sub>2</sub>O exhibits an AM configuration [54], as illustrated in Fig. 2(a). The magnetic moments localized on the Fe sites, with a magnitude of  $\sim 4 \mu_B$ , and align along the out-of-plane easy axis, resulting in a maximum value of the magnetic anisotropy energy of 7.014 meV/Fe [54]. Without SOC, monolayer Fe<sub>2</sub>Te<sub>2</sub>O belongs to the SSG No. 47.123.1.1, having the horizontal mirror  $\mathcal{M}_z = \{M_z^s || M_z^l\}$ . The sublattices with opposite spins are connected by  $\{E^s || C_{4z}^l\} \mathcal{T}$  and  $\mathcal{M}_{\bar{1}10/110} = \{C_{2,\bar{1}10/110}^s || M_{\bar{1}10/110}^l\}$ . From Eqs. (2)

and (3), one knows that  $\{E^s || C_{4z}^l\} \mathcal{T}$  would invert the eigenvalue of  $\mathcal{M}_z$ . Therefore, the electronic states connected by  $\{E^s || C_{4z}^l\} \mathcal{T}$  will have opposite both spin and  $\mathcal{M}_z$  eigenvalues, leading to the MSC.

**AM Weyl semimetal with MSC.**— The spin-resolved band structure of the monolayer Fe<sub>2</sub>Te<sub>2</sub>O without SOC is plotted in Fig. 2(c), from which two remarkable features can be observed. (i) The system exhibits an AM semi-metallic behavior, with both spin-up and spin-down channels featuring two WPs at the Fermi level. These WPs are located at the high-symmetry lines X-M and Y-M in the BZ, as illustrated in Fig. 3(b). (ii) The spin-up and spin-down states near the Fermi level are well separated from other bands and share the same eigenvalue of  $\mathcal{M}_z$ :  $m_z = i$  for spin-up states and  $m_z = -i$  for spin-down states, confirming the monolayer Fe<sub>2</sub>Te<sub>2</sub>O is an ideal MSC material.

In the spin-up channel [Fig. 2(c)], the two 2D WPs at the high-symmetry line M-X are connected by  $C_{2z} = \{C_{2z}^s || C_{2z}^l\}$ , and are protected by  $\{E^s || C_{2x}^l\}$ , as the two bands forming the WPs respectively belong to band representations  $Y_2$  and  $Y_3$ , which have opposite eigenvalues of  $\{E^s || C_{2x}^l\}$ . Since the two WPs reside around X point, we establish a symmetry-allowed  $k \cdot p$  Hamiltonian expanded from the X point and based on the band representations  $X_1^-$  and  $X_2^-$ , expressed as [54]

$$H_X = (m + t_x k_x^2 + t_y k_y^2) \sigma_z + r k_x k_y \sigma_x, \quad (4)$$

where  $\sigma$  denotes the Pauli matrices, all parameters are real, and  $k_{x(y)}$  is measured from the X point. According to the band structure, we have  $m = 0.23$  eV,  $t_x = -0.025$  eV Å<sup>2</sup>,  $t_y = -0.55$  eV Å<sup>2</sup>, and  $r = 0.42$  eV Å<sup>2</sup>. When  $\mathbf{k} = (0, \pm \sqrt{|m/t_y|}, 0)$ , the two bands cross linearly, forming two WPs  $W_{\pm}^{\uparrow}$  [see Fig. 3(b)]. The effective Hamiltonian for the WP of  $W_{\pm}^{\uparrow}$  is obtained as

$$H_{\pm}^{\uparrow} = \pm \sqrt{|m/t_y|} (2t_y k_y \sigma_z + r k_x \sigma_x), \quad (5)$$

which indeed represents a WP with linear dispersion along both  $k_x$  and  $k_y$ . The two spin-down WPs ( $W_{\pm}^{\downarrow}$ ) are connected to  $W_{\pm}^{\uparrow}$  by  $\{E^s || C_{4z}^l\} \mathcal{T}$ , and are protected by  $\{E^s || C_{2y}^l\}$ .

**MCI with MSC and quantized spin-Hall conductivity.**— In the presence of SOC, monolayer Fe<sub>2</sub>Te<sub>2</sub>O belongs to magnetic space group No. 123.4.1002, which preserves the symmetries  $\mathcal{M}_z$ ,  $C_{4z} \mathcal{T}$  and spatial inversion  $\mathcal{P}$ , but breaks  $\{E^s || C_{2x}^l\}$  and  $\{E^s || C_{2y}^l\}$ . Thus, the four 2D WPs will be gapped by SOC. Since each gapped 2D WP gives a half-integer Chern number for the valence band [58, 59], the gapped Fe<sub>2</sub>Te<sub>2</sub>O may become an insulator with nontrivial band topology.

The electronic band structure of the monolayer Fe<sub>2</sub>Te<sub>2</sub>O with SOC is shown in Fig. 2(d), where all the WPs are gapped, consistent with the symmetry analysis. However, the other remarkable feature (*i.e.* MSC) of

Fig. 2(c) persist [see Fig. 2(d)]. Specifically, while SOC induces a sizable band gap of  $\sim 0.17$  eV, it generates negligible spin hybridization, and the low-energy electrons with  $m_z = \pm i$  still exhibit opposite and (almost) perfect persistent spin polarization. Consequently, we can discuss the topology of the gapped WPs in different spin (mirror) subsystems.

Under SOC effect, the Hamiltonian (5) becomes [54]

$$\mathcal{H}_{\pm}^{\uparrow} = \pm \sqrt{|m/t_y|} (2t_y k_y \sigma_z + r k_x \sigma_x) + \Delta \sigma_y, \quad (6)$$

where  $\Delta \sigma_y$  is the mass term caused by SOC effect and  $\Delta \simeq 0.103$  eV. Particularly, the Chern number of the gapped WP is  $\frac{1}{2} \text{Sign}(t_y r \Delta)$ , which is the same for both  $\mathcal{H}_+^{\uparrow}$  and  $\mathcal{H}_-^{\uparrow}$ . This indicates that the SOC drives the spin-up ( $m_z = i$ ) channel to evolve into a Chern insulator with  $\mathcal{C}_+ = 1$ . Since the two spin channels are connected by  $C_{4z} \mathcal{T}$ , the spin-down ( $m_z = -i$ ) channel should also be a Chern insulator but with  $\mathcal{C}_- = -1$ . This is further confirmed by the Wilson loop calculations performed on the two mirror subsystems, as shown in Fig. 3(a). Therefore, the monolayer  $\text{Fe}_2\text{Te}_2\text{O}$  with SOC is an MCI with a mirror Chern number of  $\mathcal{C}_m = (\mathcal{C}_+ - \mathcal{C}_-)/2 = 1$ . To the best of our knowledge, monolayer  $\text{Fe}_2\text{Te}_2\text{O}$  is the first material candidate for a magnetic MCI.

A hallmark of MCI is the presence of topological gapless edge states, which have opposite mirror eigenvalues. In Fig. 3(c), we plot the spectrum of a nanoribbon along  $(1\bar{1}0)$  direction constructed by the monolayer  $\text{Fe}_2\text{Te}_2\text{O}$  with SOC. Two counter-propagating edge states appear in the bulk gap, which intersects linearly at the  $\bar{\Gamma}$  point. Interestingly, these two edge states are almost entirely contributed by the spin-up and spin-down electrons [see Fig. 3(c)]. While the system has SOC, the hybridization of the spin-up and spin-down of the edge states is always negligible, even in the region where the two states are close. This is caused by the MSC. Without MSC, the spin polarization of the edge states is not persistent, but varies with the momentum.

Using a four-terminal measurement setup, we study the spin transport of the monolayer  $\text{Fe}_2\text{Te}_2\text{O}$ . The result is shown in Fig. 3(d). One observes that the spin-Hall conductivity of the system is quantized to the well-known constant  $e/(4\pi)$  in the bulk gap. Therefore, we demonstrate that via the MSC, a quantized spin-Hall conductivity is achieved in an MCI rather than a QSH insulator.

**Discussion.**— In this work, we have proposed a new coupling effect to realize quantized spin-Hall conductivity. The underneath physics shifts the search for QSH insulators to magnetic MCIs with MSC.

We highlight the robustness of the topological edge states in Fig. 3(c). The  $\Gamma$ - $M$  path in the bulk BZ corresponds to an effective 1D system, which have three mirrors:  $\mathcal{M}_z$ ,  $\mathcal{M}_{110}$ , and  $\mathcal{M}_{1\bar{1}0}$ . Due to  $\mathcal{M}_{1\bar{1}0}$ , the 1D system can be classified by a  $Z_2$  topological index, *i.e.* the Zak phase. Moreover, the Zak phase can be fur-

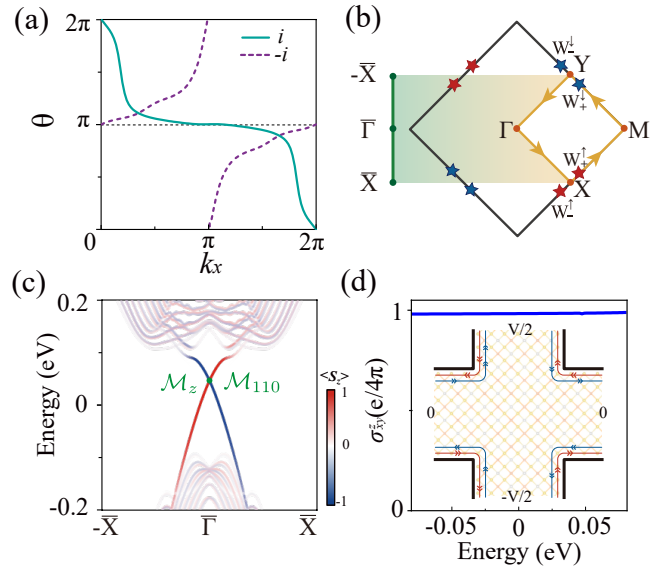


FIG. 3. (a) Wilson loops of the  $\text{Fe}_2\text{Te}_2\text{O}$  with SOC, which are obtained in the two  $\mathcal{M}_z$  ( $\mathcal{M}_z = \pm i$ ) subsystems, respectively. (b) Bulk and edge BZs. The location of the four AM WPs in  $\text{Fe}_2\text{Te}_2\text{O}$  without SOC are presented in bulk BZ. (c) The spectrum of the nanoribbon with  $(1\bar{1}0)$  edges. The colors denote the out-of-plane spin polarization. The topological edge states exhibit an almost 100% spin polarization. The band crossing of the edge states at  $\bar{\Gamma}$  point is doubly protected by  $\mathcal{M}_z$  and  $\mathcal{M}_{110}$ . (d) The spin-Hall conductivity  $\sigma_{xy}^z$  in the bulk band gap, obtained by a four-terminal measurement setup. Due to the almost perfect spin polarization of the edge states, the spin-Hall conductivity  $\sigma_{xy}^z$  is quantized to the expected constant  $e/(4\pi)$ .

ther respectively calculated in the two  $\mathcal{M}_{110}$ -invariant subsystems. Interestingly, a detailed calculation shows that the Zak phases of the  $\Gamma$ - $M$  path in the two  $\mathcal{M}_{110}$ -invariant subsystems are nontrivial, leading to two degenerate topological boundary states at the boundary, which exactly the  $\bar{\Gamma}$  point in Fig. 3(c). Thus, the gapless point at  $\bar{\Gamma}$  is doubly protected by  $\mathcal{M}_z$  and  $\mathcal{M}_{110}$ , and then should be robust against the  $\mathcal{M}_z$ -breaking perturbations.

Furthermore, the band gap of monolayer  $\text{Fe}_2\text{Te}_2\text{O}$  with SOC is about 0.17 eV, which is much larger than the thermal energy at room temperature ( $\sim 26$  meV). This suggests that the quantized spin-Hall conductivity can be observed at room-temperature, making the system promising for the design of room temperature devices.

Finally, we would like to point out that the search for realistic (SOC) materials with persistent spin polarization is an important and active topic in the field of spintronics [48–53]. The MSC provides an alternative mechanism to realize it.

\* These authors contributed equally to this work.

† [zhiming\\_yu@bit.edu.cn](mailto:zhiming_yu@bit.edu.cn)

‡ [ygyao@bit.edu.cn](mailto:ygyao@bit.edu.cn)

- [1] K. S. Novoselov, A. K. Geim, S. V. Morozov, D. Jiang, M. I. Katsnelson, I. V. Grigorieva, S. V. Dubonos, and A. A. Firsov, Two-dimensional gas of massless dirac fermions in graphene, *Nature* **438**, 197 (2005).
- [2] K. F. Mak, C. Lee, J. Hone, J. Shan, and T. F. Heinz, Atomically thin mos<sub>2</sub>: a new direct-gap semiconductor, *Phys. Rev. Lett.* **105**, 136805 (2010).
- [3] L. Li, Y. Yu, G. J. Ye, Q. Ge, X. Ou, H. Wu, D. Feng, X. H. Chen, and Y. Zhang, Black phosphorus field-effect transistors, *Nat. Nanotechnol.* **9**, 372 (2014).
- [4] C.-C. Liu, W. Feng, and Y. Yao, Quantum spin hall effect in silicene and two-dimensional germanium, *Phys. Rev. Lett.* **107**, 076802 (2011).
- [5] J. Zhao, H. Liu, Z. Yu, R. Quhe, S. Zhou, Y. Wang, C. C. Liu, H. Zhong, N. Han, J. Lu, *et al.*, Rise of silicene: A competitive 2d material, *Prog. Mater. Sci.* **83**, 24 (2016).
- [6] Y. Xu, B. Yan, H.-J. Zhang, J. Wang, G. Xu, P. Tang, W. Duan, and S.-C. Zhang, Large-gap quantum spin hall insulators in tin films, *Phys. Rev. Lett.* **111**, 136804 (2013).
- [7] F. Reis, G. Li, L. Dudy, M. Bauernfeind, S. Glass, W. Hanke, R. Thomale, J. Schäfer, and R. Claessen, Bismuthene on a sic substrate: A candidate for a high-temperature quantum spin hall material, *Science* **357**, 287 (2017).
- [8] C. Gong, L. Li, Z. Li, H. Ji, A. Stern, Y. Xia, T. Cao, W. Bao, C. Wang, Y. Wang, *et al.*, Discovery of intrinsic ferromagnetism in two-dimensional van der waals crystals, *Nature* **546**, 265 (2017).
- [9] C.-Z. Chang, J. Zhang, X. Feng, J. Shen, Z. Zhang, M. Guo, K. Li, Y. Ou, P. Wei, L.-L. Wang, *et al.*, Experimental observation of the quantum anomalous hall effect in a magnetic topological insulator, *Science* **340**, 167 (2013).
- [10] P. Li, Y. Wen, X. He, Q. Zhang, C. Xia, Z.-M. Yu, S. A. Yang, Z. Zhu, H. N. Alshareef, and X.-X. Zhang, Evidence for topological type-ii weyl semimetal wte<sub>2</sub>, *Nat. Commun.* **8**, 2150 (2017).
- [11] Y. Deng, Y. Yu, M. Z. Shi, Z. Guo, Z. Xu, J. Wang, X. H. Chen, and Y. Zhang, Quantum anomalous hall effect in intrinsic magnetic topological insulator mnbi<sub>2</sub>te<sub>4</sub>, *Science* **367**, 895 (2020).
- [12] J. Li, Y. Li, S. Du, Z. Wang, B.-L. Gu, S.-C. Zhang, K. He, W. Duan, and Y. Xu, Intrinsic magnetic topological insulators in van der waals layered mnbi<sub>2</sub>te<sub>4</sub>-family materials, *Sci. Adv.* **5**, eaaw5685 (2019).
- [13] F. De Juan, A. G. Grushin, T. Morimoto, and J. E. Moore, Quantized circular photogalvanic effect in weyl semimetals, *Nat. Commun.* **8**, 15995 (2017).
- [14] Y. Liu, Z.-M. Yu, C. Xiao, and S. A. Yang, Quantized circulation of anomalous shift in interface reflection, *Phys. Rev. Lett.* **125**, 076801 (2020).
- [15] L. Li, C. Cui, R.-W. Zhang, Z.-M. Yu, and Y. Yao, Planar hall plateau in magnetic weyl semimetals, *Sci. Bull.* **70**, 187 (2025).
- [16] B. A. Bernevig, Topological insulators and topological superconductors, in *Topological Insulators and Topological Superconductors* (Princeton university press, 2013).
- [17] J. Maciejko, T. L. Hughes, and S.-C. Zhang, The quantum spin hall effect, *Annu. Rev. Condens. Matter Phys.* **2**, 31 (2011).
- [18] M. Z. Hasan and C. L. Kane, Colloquium: topological insulators, *Rev. Mod. Phys.* **82**, 3045 (2010).
- [19] X.-L. Qi and S.-C. Zhang, Topological insulators and superconductors, *Rev. Mod. Phys.* **83**, 1057 (2011).
- [20] C. L. Kane and E. J. Mele, Z<sub>2</sub> topological order and the quantum spin hall effect, *Phys. Rev. Lett.* **95**, 146802 (2005).
- [21] B. A. Bernevig, T. L. Hughes, and S.-C. Zhang, Quantum spin hall effect and topological phase transition in hgte quantum wells, *science* **314**, 1757 (2006).
- [22] J.-Y. Zou, B. Fu, and S.-Q. Shen, Topological properties of c<sub>4z</sub>t-symmetric semimetals, *Communications Physics* **7**, 275 (2024).
- [23] D. S. Antonenko, R. M. Fernandes, and J. W. Venderbos, Mirror chern bands and weyl nodal loops in altermagnets, *arXiv:2402.10201* (2024).
- [24] L. Šmejkal, R. González-Hernández, T. Jungwirth, and J. Sinova, Crystal time-reversal symmetry breaking and spontaneous hall effect in collinear antiferromagnets, *Sci. Adv.* **6**, eaaz8809 (2020).
- [25] R. González-Hernández, L. Šmejkal, K. Věborný, Y. Yahagi, J. Sinova, T. Jungwirth, and J. Železný, Efficient electrical spin splitter based on nonrelativistic collinear antiferromagnetism, *Phys. Rev. Lett.* **126**, 127701 (2021).
- [26] L. Šmejkal, J. Sinova, and T. Jungwirth, Beyond conventional ferromagnetism and antiferromagnetism: A phase with nonrelativistic spin and crystal rotation symmetry, *Phys. Rev. X* **12**, 031042 (2022).
- [27] L. Šmejkal, J. Sinova, and T. Jungwirth, Emerging research landscape of altermagnetism, *Phys. Rev. X* **12**, 040501 (2022).
- [28] L. Šmejkal, A. B. Hellenes, R. González-Hernández, J. Sinova, and T. Jungwirth, Giant and tunneling magnetoresistance in unconventional collinear antiferromagnets with nonrelativistic spin-momentum coupling, *Phys. Rev. X* **12**, 011028 (2022).
- [29] H.-Y. Ma, M. Hu, N. Li, J. Liu, W. Yao, J.-F. Jia, and J. Liu, Multifunctional antiferromagnetic materials with giant piezomagnetism and noncollinear spin current, *Nat. Commun.* **12**, 2846 (2021).
- [30] D.-F. Shao, Y.-Y. Jiang, J. Ding, S.-H. Zhang, Z.-A. Wang, R.-C. Xiao, G. Gurung, W. Lu, Y. Sun, and E. Y. Tsybal, Néel spin currents in antiferromagnets, *Phys. Rev. Lett.* **130**, 216702 (2023).
- [31] L. Bai, W. Feng, S. Liu, L. Šmejkal, Y. Mokrousov, and Y. Yao, Altermagnetism: Exploring new frontiers in magnetism and spintronics, *Adv. Funct. Mater.* **34**, 2409327 (2024).
- [32] H. Bai, L. Han, X. Y. Feng, Y. J. Zhou, R. X. Su, Q. Wang, L. Y. Liao, W. X. Zhu, X. Z. Chen, F. Pan, X. L. Fan, and C. Song, Observation of spin splitting torque in a collinear antiferromagnet ruo<sub>2</sub>, *Phys. Rev. Lett.* **128**, 197202 (2022).
- [33] S. Lee, S. Lee, S. Jung, J. Jung, D. Kim, Y. Lee, B. Seok, J. Kim, B. G. Park, L. Šmejkal, *et al.*, Broken kramers degeneracy in altermagnetic mn<sub>2</sub>, *Phys. Rev. Lett.* **132**, 036702 (2024).
- [34] P.-J. Guo, Z.-X. Liu, and Z.-Y. Lu, Quantum anomalous hall effect in collinear antiferromagnetism, *npj Comput. Mater.* **9**, 70 (2023).

- [35] P.-J. Guo, Y. Gu, Z.-F. Gao, and Z.-Y. Lu, Altermagnetic ferroelectric  $\text{LiFe}_2\text{F}_6$  and spin-triplet excitonic insulator phase, arXiv:2312.13911 (2023).
- [36] P.-J. Guo, X.-Y. Hou, Z.-F. Gao, H.-C. Yang, W. Ji, and Z.-Y. Lu, Luttinger compensated bipolarized magnetic semiconductor, arXiv:2502.18136 (2025).
- [37] R.-W. Zhang, C. Cui, R. Li, J. Duan, L. Li, Z.-M. Yu, and Y. Yao, Predictable gate-field control of spin in altermagnets with spin-layer coupling, Phys. Rev. Lett. **133**, 056401 (2024).
- [38] T. He, L. Li, C. Cui, R.-W. Zhang, Z.-M. Yu, G. Liu, and X. Zhang, Quasi-one-dimensional spin transport in altermagnetic  $z_3$  nodal net metals, Phys. Rev. Lett. **133**, 146602 (2024).
- [39] Y. Liu, J. Yu, and C.-C. Liu, Twisted magnetic van der waals bilayers: an ideal platform for altermagnetism, Phys. Rev. Lett. **133**, 206702 (2024).
- [40] M. Gu, Y. Liu, H. Zhu, K. Yananose, X. Chen, Y. Hu, A. Stroppa, and Q. Liu, Ferroelectric switchable altermagnetism, arXiv:2411.14216 (2024).
- [41] W. Sun, H. Ye, L. Liang, N. Ding, S. Dong, and S.-S. Wang, Stacking-dependent ferroicity of a reversed bilayer: Altermagnetism or ferroelectricity, Phys. Rev. B **110**, 224418 (2024).
- [42] W. Brinkman and R. J. Elliott, Theory of spin-space groups, Proc. R. Soc. A **294**, 343 (1966).
- [43] D. B. Litvin and W. Opechowski, Spin groups, Physica (Utrecht) **76**, 538 (1974).
- [44] W. Brinkman and R. Elliott, Space group theory for spin waves, J. Appl. Phys. **37**, 1457 (1966).
- [45] Z. Xiao, J. Zhao, Y. Li, R. Shindou, and Z.-D. Song, Spin space groups: Full classification and applications, Phys. Rev. X **14**, 031037 (2024).
- [46] X. Chen, J. Ren, Y. Zhu, Y. Yu, A. Zhang, P. Liu, J. Li, Y. Liu, C. Li, and Q. Liu, Enumeration and representation theory of spin space groups, Phys. Rev. X **14**, 031038 (2024).
- [47] Y. Jiang, Z. Song, T. Zhu, Z. Fang, H. Weng, Z.-X. Liu, J. Yang, and C. Fang, Enumeration of spin-space groups: Toward a complete description of symmetries of magnetic orders, Phys. Rev. X **14**, 031039 (2024).
- [48] J. Schliemann, Colloquium: Persistent spin textures in semiconductor nanostructures, Rev. Mod. Phys. **89**, 011001 (2017).
- [49] L. Tao and E. Y. Tsymbal, Persistent spin texture enforced by symmetry, Nat. Commun. **9**, 2763 (2018).
- [50] H. J. Zhao, H. Nakamura, R. Arras, C. Paillard, P. Chen, J. Gosteau, X. Li, Y. Yang, and L. Bellaiche, Purely cubic spin splittings with persistent spin textures, Phys. Rev. Lett. **125**, 216405 (2020).
- [51] J. H. Garcia, M. Vila, C.-H. Hsu, X. Waintal, V. M. Pereira, and S. Roche, Canted persistent spin texture and quantum spin hall effect in  $\text{wTe}_2$ , Phys. Rev. Lett. **125**, 256603 (2020).
- [52] M. Król, K. Rechcińska, H. Sigurdsson, P. Oliwa, R. Mazur, P. Morawiak, W. Piecek, P. Kula, P. G. Lagoudakis, M. Matuszewski, *et al.*, Realizing optical persistent spin helix and stern-gerlach deflection in an anisotropic liquid crystal microcavity, Phys. Rev. Lett. **127**, 190401 (2021).
- [53] J. Tian, S. Hong, I. Miotkowski, S. Datta, and Y. P. Chen, Observation of current-induced, long-lived persistent spin polarization in a topological insulator: A rechargeable spin battery, Sci. Adv. **3**, e1602531 (2017).
- [54] See Supplemental Material for the methods, corresponding informations of monolayer  $\text{Fe}_2\text{Te}_2\text{O}$  including exfoliation energy, stability, magnetic ground state, topological properties, etc.
- [55] F. Takeiri, Y. Matsumoto, T. Yamamoto, N. Hayashi, Z. Li, T. Tohyama, C. Tassel, C. Ritter, Y. Narumi, M. Hagiwara, *et al.*, High-pressure synthesis of the layered iron oxyselenide  $\text{baf}_2\text{se}_2\text{o}$  with strong magnetic anisotropy, Phys. Rev. B **94**, 184426 (2016).
- [56] S.-J. Song, J.-Y. Lu, Q.-Q. Zhu, Z. Ren, and G.-H. Cao, Crystal structure and physical properties of layered  $\text{na}_2\text{fe}_2\text{s}_2\text{o}$ , J. Phys. Chem. Solids **181**, 111469 (2023).
- [57] J. He, D. Wang, H. Shi, H. Yang, J. Li, and G. Chen, Synthesis, structure, and magnetic properties of the layered iron oxychalcogenide  $\text{na}_2\text{fe}_2\text{se}_2\text{o}$ , Phys. Rev. B **84**, 205212 (2011).
- [58] W. Yao, S. A. Yang, and Q. Niu, Edge states in graphene: From gapped flat-band to gapless chiral modes, Phys. Rev. Lett. **102**, 096801 (2009).
- [59] D.-P. Liu, Z.-M. Yu, and Y.-L. Liu, Pure spin current and perfect valley filter by designed separation of the chiral states in two-dimensional honeycomb lattices, Phys. Rev. B **94**, 155112 (2016).